ARMY RESEARCH LABORATORY

The Influence of Novel Alloying Additions on the Performance of Magnesium Alloy AZ31B

by Kateryna Gusieva, Nick Birbilis, Vincent H. Hammond, Joseph P. Labukas, and Brian E. Placzankis

ARL-MR-856 **November 2013**

NOTICES

Disclaimers

The findings in this report are not to be construed as an official Department of the Army position unless so designated by other authorized documents.

Citation of manufacturer's or trade names does not constitute an official endorsement or approval of the use thereof.

Destroy this report when it is no longer needed. Do not return it to the originator.

Army Research Laboratory
Aberdeen Proving Ground, MD 21005-5069

ARL-MR-856 **November 2013**

The Influence of Novel Alloying Additions on the Performance of Magnesium Alloy AZ31B

Kateryna Gusieva and Nick Birbilis
Department of Materials Engineering, Monash University (Australia)

Vincent H. Hammond, Joseph P. Labukas, and Brian E. Placzankis
Weapons and Materials Research Directorate, ARL

REPORT DOCUMENTATION PAGE

Form Approved
OMB No. 0704-0188

1. REPORT DATE *(DD-MM-YYYY)*	2. REPORT TYPE	3. DATES COVERED (From - To)
November 2013	Final	October 2012–September 2013

4. TITLE AND SUBTITLE
The Influence of Novel Alloying Additions on the Performance of Magnesium Alloy AZ31B

5a. CONTRACT NUMBER
W911NF-13-2-0007

5b. GRANT NUMBER

5c. PROGRAM ELEMENT NUMBER

6. AUTHOR(S)
Kateryna Gusieva,* Nick Birbilis,* Vincent H. Hammond, Joseph P. Labukas, and Brian E. Placzankis

5d. PROJECT NUMBER

5e. TASK NUMBER

5f. WORK UNIT NUMBER

7. PERFORMING ORGANIZATION NAME(S) AND ADDRESS(ES)
U.S. Army Research Laboratory
ATTN: RDRL-WMM-F
Aberdeen Proving Ground, MD 21005-5069

8. PERFORMING ORGANIZATION REPORT NUMBER
ARL-MR-856

9. SPONSORING/MONITORING AGENCY NAME(S) AND ADDRESS(ES)

10. SPONSOR/MONITOR'S ACRONYM(S)

11. SPONSOR/MONITOR'S REPORT NUMBER(S)

12. DISTRIBUTION/AVAILABILITY STATEMENT
Approved for public release; distribution unlimited.

13. SUPPLEMENTARY NOTES
*Monash University, Melbourne, Australia.

14. ABSTRACT
Due to their low density, magnesium (Mg) alloys are of interest for their potential in achieving significant lightweighting of vehicular platforms. Because many of the current Mg alloys are based on a rather small group of alloying elements, there are often limited differences between them in properties (strength, corrosion resistance, etc.). In an attempt to develop new alloys that display appreciable improvements in overall performance, a series of alloys incorporating nontraditional alloying elements have been synthesized and evaluated for mechanical and electrochemical response. To facilitate insight into the influence of the respective alloying addition(s), a relatively simple Mg alloy (AZ31B) was chosen as the baseline material. Because this alloy has been extensively characterized, any improvements or reductions in performance should be more easily attributed to the alloying additions. The key metrics used, on both an individual and collective basis, to evaluate the influence of alloying additions were strength, microstructural texture, and corrosion resistance. This report provides a brief synopsis of the results obtained in the first year of this three-year effort.

15. SUBJECT TERMS
magnesium, alloying, mechanical properties, corrosion, microscopy

16. SECURITY CLASSIFICATION OF:			17. LIMITATION OF ABSTRACT	18. NUMBER OF PAGES	19a. NAME OF RESPONSIBLE PERSON
a. REPORT	b. ABSTRACT	c. THIS PAGE			Vincent H. Hammond
Unclassified	Unclassified	Unclassified	UU	24	19b. TELEPHONE NUMBER (*Include area code*) 410-306-4961

Contents

List of Figures

List of Tables

1. Background

The research effort discussed herein is the result of conversations with Professor Nick Birbilis of Monash University, Australia, during one of his recent visits to the U.S. Army Research Laboratory (ARL). Initially, the discussions focused on ways to improve the corrosion resistance of magnesium (Mg) alloys to increase the potential usefulness of these alloys to the U.S. Army. As the discussions continued, however, it became apparent that the project offered an opportunity to simultaneously improve both mechanical and electrochemical performance of Mg through the selective choice of elemental additions. To limit the scope of the project, the decision was made to focus solely on alloy AZ31B. This decision was made for two reasons: (1) AZ31B is a "simple" alloy in which the effect of alloying additions would be readily observed, and (2) this alloy has already been specified for potential use as an armor plate material.[1] The approach used in the study draws extensively on the prior knowledge generated by Professor Birbilis and others at Monash regarding the influence of atypical alloying elements on the behavior of Mg alloys. As a result, significant and noteworthy observations have been achieved in the first year of the project.

2. Introduction

To date, the majority of Mg alloys have used a rather small group of alloying elements (such as aluminum [Al], zinc [Zn], and zirconium [Zr]) in varying amounts and/or ratios. As a result, there have been only limited improvements in performance. More recently, alloys using a variety of the rare earth elements have been developed. Typically, these alloys have shown significant improvements in mechanical properties and to a lesser degree in corrosion performance. However, rare earth elements are often costly and heavier than Mg. Thus, depending on the amount used in the alloy, there can be an appreciable increase in overall cost and density of the final alloy product. In many cases, the addition of alloying elements often results in only one property of interest (e.g., strength, corrosion performance, toughness, etc.) being significantly enhanced while the others are only minimally improved or, in the worst-case scenario, actually lowered to an undesirable level.

In an effort to create Mg alloys in which the total combination of properties is improved, a series of alloys incorporating nontraditional alloying elements have been synthesized and evaluated for mechanical and electrochemical performance. In particular, the goal was to identify elements that offered the best combination of increased strength, reduced texture, and improved durability (e.g., corrosion resistance). In selecting the alloying elements, their solubility in Mg was a

[1] MIL-DTL-32333 (MR). *Armor Plate, Magnesium Alloy, AZ31B, Appliqué* **2009**.

key criterion, so that potential strength increase from grain size reduction and/or solid solution strengthening would occur. Moreover, it was also desired that the element have a lower dissolution rate than Mg so that improvements in corrosion performance could be realized. Consideration was also given to atomic radius, as it has been shown that larger atoms can reduce the degree of texture observed in Mg alloys. Using these criteria, the following elements were selected: indium (In), bismuth (Bi), strontium (Sr), Zr, titanium (Ti), calcium (Ca), lithium (Li), yttrium (Y,) lanthanum (La), neodymium (Nd), scandium (Sc), lutetium (Lu), silver (Ag), and arsenic (As).

To accurately determine the influence of the alloying addition, a relatively simple Mg alloy (AZ31B) was chosen as the baseline material. AZ31B is a solid-solution-strengthened alloy with minimal precipitate content. Moreover, the mechanical and electrochemical performance of the alloy has been well characterized. As such, it was thought that any improvements, or reductions, in performance could be easily traced to the effects of the alloying additions.

3. Experimental Approach

Alloys studied in this effort were produced by adding the desired amount of the respective alloying element(s) to a molten stock of commercially available AZ31B ingots. The alloy was held at 730 °C for 30 min, during which it was intermittently stirred to ensure mixing of the additions into the melt. The melt was then poured into a preheated (250 °C) steel mold and allowed to cool to room temperature.

The as-cast rectangular ingots were machined into 32-mm-diameter cylindrical billets prior to direct extrusion at 400 °C using a manually operated 100-ton vertical hydraulic press. The cylindrical billet was placed into a preheated tool steel die and extruded through an 8-mm-diameter die at constant load. The rods were extruded directly into water to prevent any phase transformations occurring during a slow cool-down from the extrusion temperature.

Compositional analysis of the alloys was performed using inductively coupled plasma-atomic emission spectrometry. Scanning electron microscopy (SEM) was used to examine the microstructures of the as-cast and extruded alloys for second phases and/or precipitates. Optical microscopy was used to determine grain-size distribution. Tensile properties were determined using dog-bone specimens with a 4-mm diameter and 16-mm gage length cut from the longitudinal section of the extruded bars. Tests were performed at room temperature using a cross-head speed of approximately 1 mm/min. Six tests were performed per alloy composition. Texture analysis was similarly performed on longitudinal sections of extruded samples using an

x-ray diffractometer. The collected raw data was processed using the Resmat TexTool, with pole figures constructed using MatLab software.

Samples for electrochemical testing were cut from extruded bars. Prior to testing, the outer surface was removed to avoid any possible iron contamination resulting from the extrusion process. The potentiodynamic polarization tests were carried out in 0.1-M sodium chloride (NaCl) electrolyte using a standard electrochemical "flat-cell" that included a saturated calomel reference electrode and a Ti-mesh counter electrode. The open circuit potential was measured for 10 min prior to polarization to determine a stable potential. The polarizations were performed using a sweep rate of 1 mV/s and conducted at least six times. The polarization curves were used to determine the corrosion current via a Tafel-type fit using EC-Lab software. Mass loss tests were carried out in triplicate for 24 h at room temperature on cylindrical samples ground down to 1200-grit silicon-carbide paper. The dimensions and weight of the samples were measured prior to immersion in 170 ml of 0.1-M NaCl solution. After exposure, silver chromate solution was used to remove the corrosion product, after which the weight of the corroded sample was measured.

4. Results

The results of compositional analysis for all of the produced alloys are given in table 1. In general, the content of the major alloying elements (Al, Zn, [manganese] Mn) of the alloys was in reasonably good agreement with the standard composition. The AZ31B baseline alloy was created by melting, casting, and extruding a commercially supplied AZ31B alloy ingot. As such, it provides a fully reasonable baseline by which to evaluate the modified alloys.

Table 1. Composition of the alloys investigated in this study. Also provided are the allowable ranges for Al, Zn, Mn, and Fe.

Alloy	Al	Zn	Mn	Fe	Zr	Other Elements
AZ31B	3.28	0.86	0.38	0.01	<0.005	Cast at Monash
AZ31-In	3.0	0.87	0.4	0.006	0	0.46 In
AZ31-Bi	3.15	0.87	0.43	0.01	0	0.48 Bi
AZ31-Sr	3.12	0.89	0.14	0.012	0	0.047 Sr
AZ31-Ti	3.15	0.87	0.19	0.093	0	0.048 Ti
AZ31-RE	3.13	0.92	0.37	0.008	0	0.23 La, 0.087 Nd, <0.005 Y
AZ31-Li	3.33	0.89	0.35	0.007	0	0.88 Li
AZ31-Bi,Nd	2.95	0.85	0.39	0.01	0	0.19 Nd, 0.53 Bi
AZ31-Ca	2.6	0.74	0.39	0.032	0	0.1 Ca
AZ31-Y	3.09	0.88	0.35	0.006	0	0.99 Y
AZ31-Sc	2.78	0.91	0.32	0.003	0	0.1 Sc, <0.01 Lu
AZ31-Ag	3.3	0.87	0.37	0.013	0.005	0.075 Ag
AZ31-Lu	3.05	0.91	0.36	0.002	0	0.21 Lu, <0.01 Sc
AZ31-As	3.24	0.85	0.37	0.004	<0.005	<0.005 As, <0.005 Ag
Allowable Range	2.5–3.5	0.7–1.3	0.2–1.0	0.004 Max	—	—

Note: Fe = iron; RE = rare earth.

SEM micrograph and energy-dispersive x-ray (EDX) results for selected alloys are shown in figures 1a–e. Such data is useful in determining if the addition of the minor alloying elements has altered the presence/type of precipitates and/or second phases typically associated with AZ31B. For example, results for AZ31B shown in figure 1a reveal the typical "swirl"-like pattern for this alloy that is composed of primary α-Mg enriched with Al. In addition, the presence of several precipitates—AlMnFe, Al_4Mn, and $Mg_{17}Al_{12}$—in the Mg matrix grains is also clearly seen. Examples of the influence of alloying element on the microstructure are given in the other four results. Because the Bi content was below the solid solubility limit, it can be seen that all of the added Bi went into solid solution with minimal impact on the "swirl" pattern as well as the typical precipitate formation. Micrographs for the other three example alloys reveal dramatic changes in both the base microstructural features as well as precipitate composition. For the Y-modified alloy, it appears that an AlMgY phase formed, with the apparent result that the solute became Al-poor, thereby resulting in reduced strength and increased corrosion rates (as seen in the following sections). For the BiNd and Sc alloys, it appears that the added alloying element is primarily found in AlMnFe-type (Fe = iron) or Al-based precipitates (such as Al_3Sc). In addition, in the Y and BiNd alloys, it appears that Fe is now present more in solid solution than in the precipitates. Analysis is ongoing to fully identify precipitates and/or second phases in the modified alloys and any resulting changes in physical or electrochemical properties.

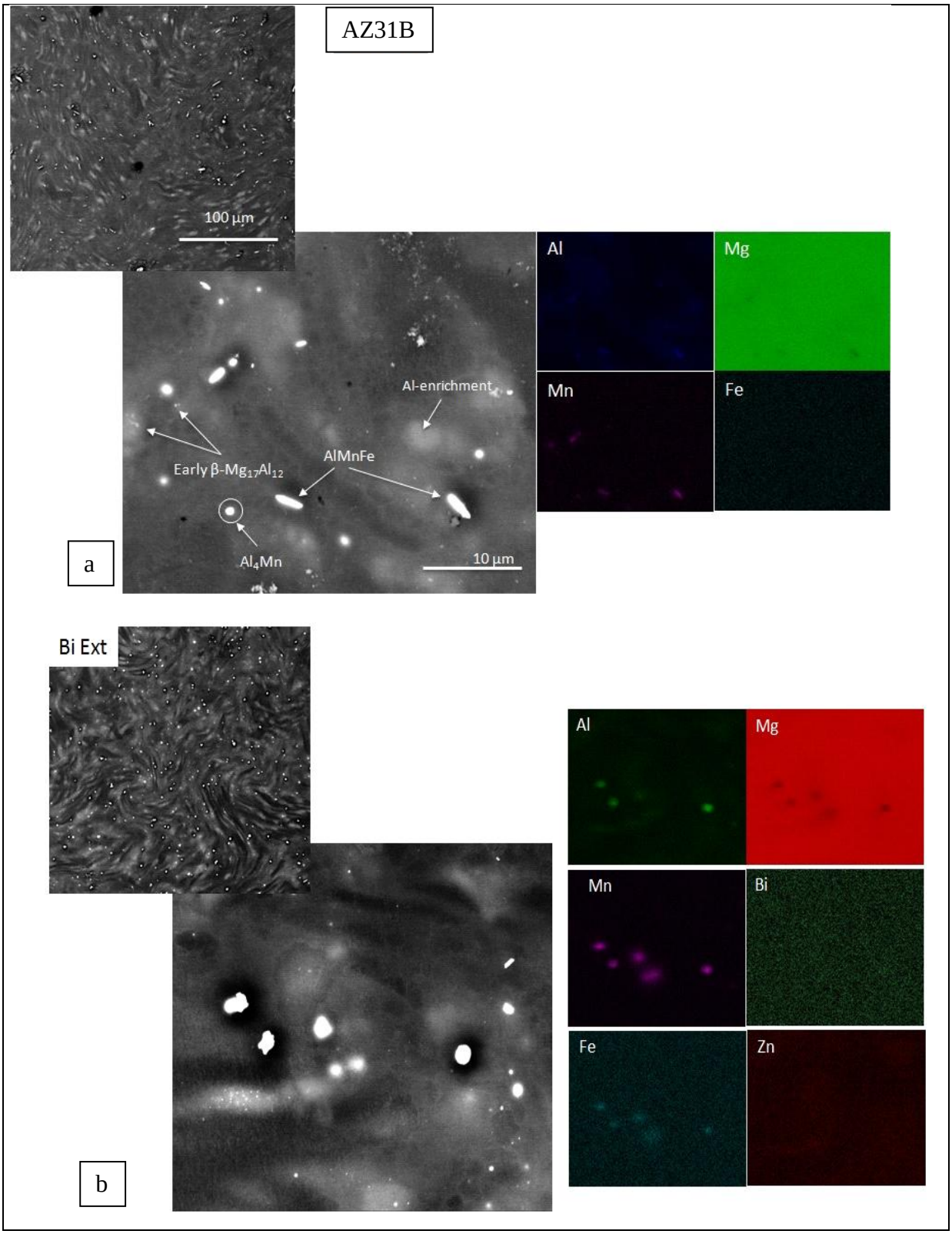

Figure 1. SEM micrographs and corresponding EDX results for selected alloys: (a) base AZ31B and (b) Bi-modified.

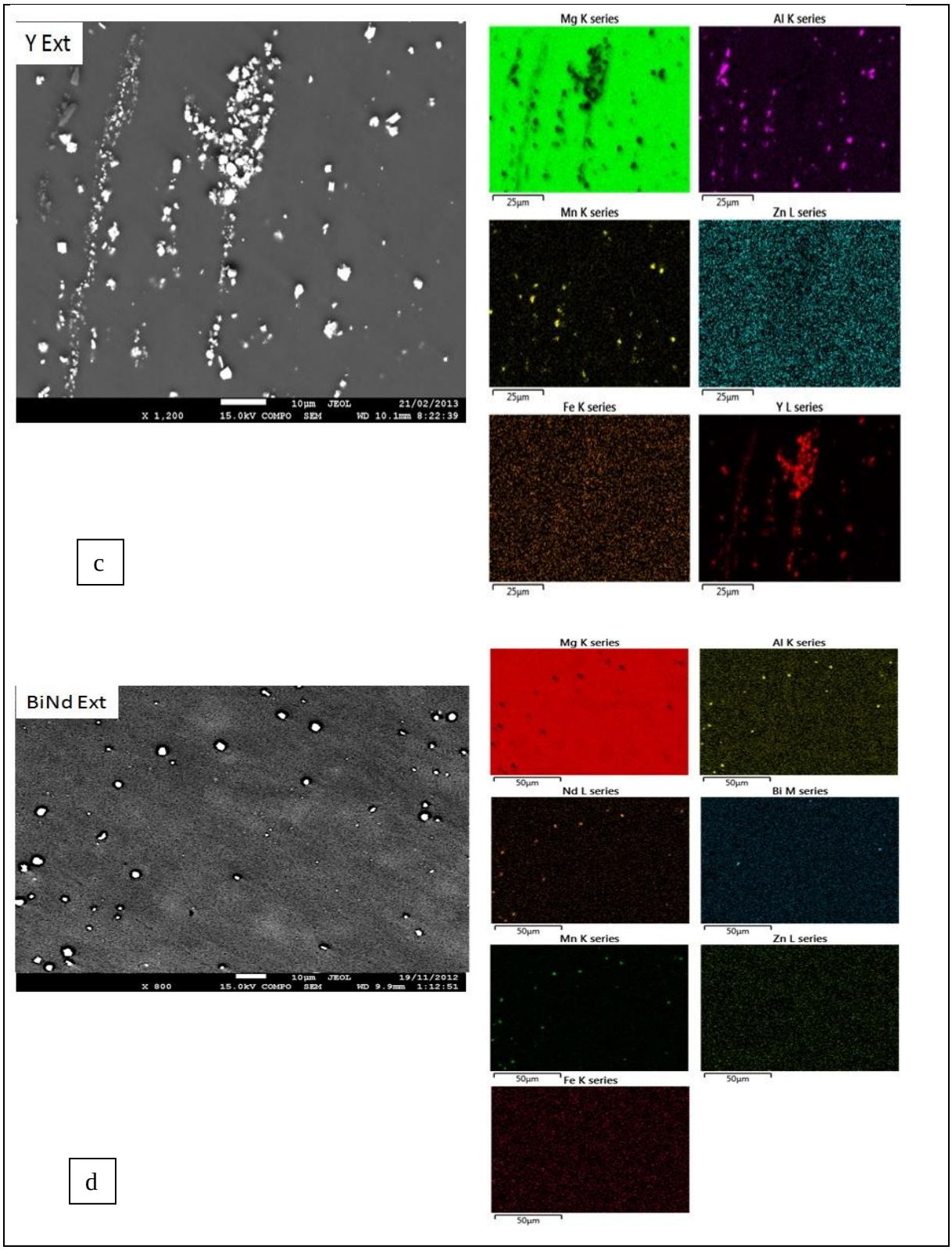

Figure 1. SEM micrographs and corresponding EDX results for selected alloys: (c) Y-modified and (d) BiNd-modified (continued).

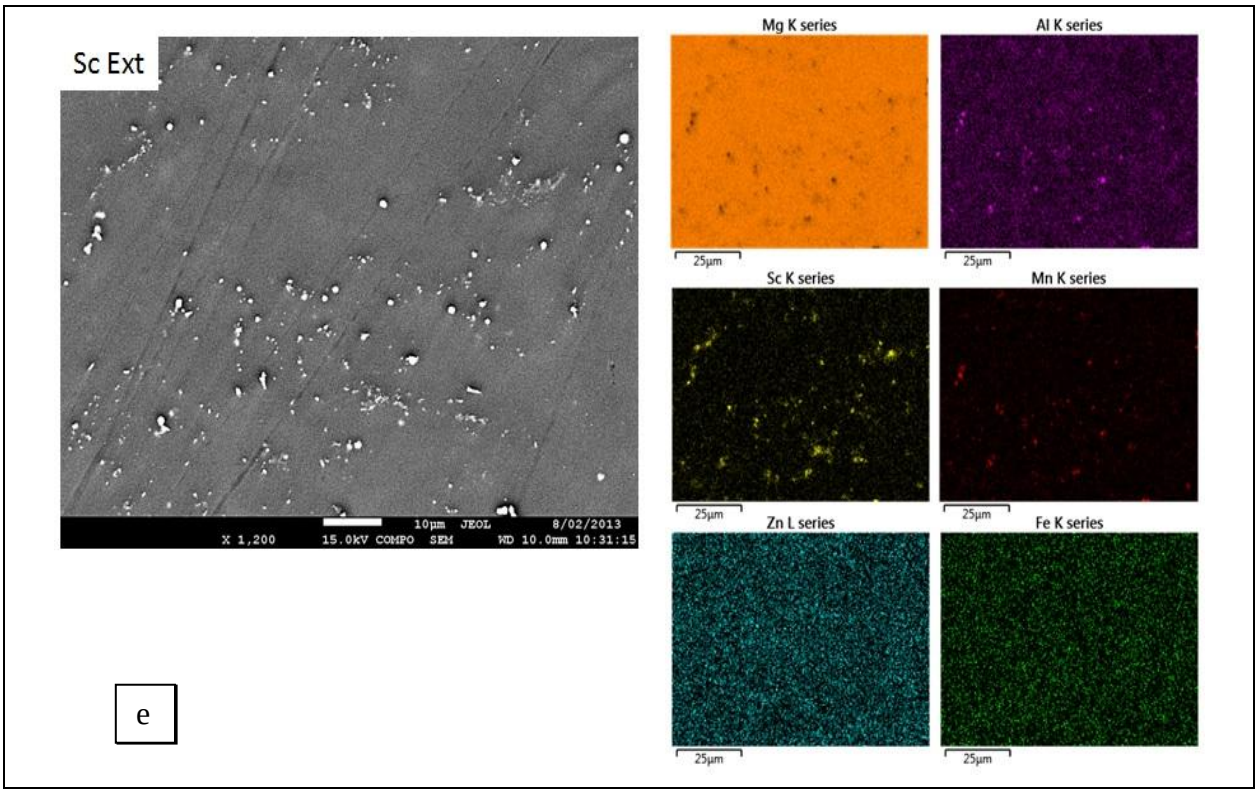

Figure 1. SEM micrographs and corresponding EDX results for selected alloys: (e) Sc-modified (continued).

Shown in figures 2(a–d) and 3(a–d) are representative micrographs from some of the as-cast and extruded alloys. In the majority of alloys, the addition of another minor alloying element resulted in a grain-size reduction relative to the "parent" AZ31B alloy in the as-cast condition. As could be expected, the results from the extruded alloys are not as clear-cut as those for the as-cast alloys. The microstructure of the extruded AZ31B alloy consists of both large unrecrystallized and fine recrystallized grains. The majority of the recrystallized grains are embedded between elongated bands of the unrecrystallized grains. Depending on the addition, the alloyed AZ31B samples can be similar in appearance or consist of mostly medium and fine grains, with only a small number of large grains. It appears that the pattern in grain-size distributions can be traced back to the grain-boundary density of the as-cast alloys. That is, those with the highest grain-boundary density (smaller grain size) in the as-cast condition had the more homogeneous, fine-grained microstructure in the extruded condition.

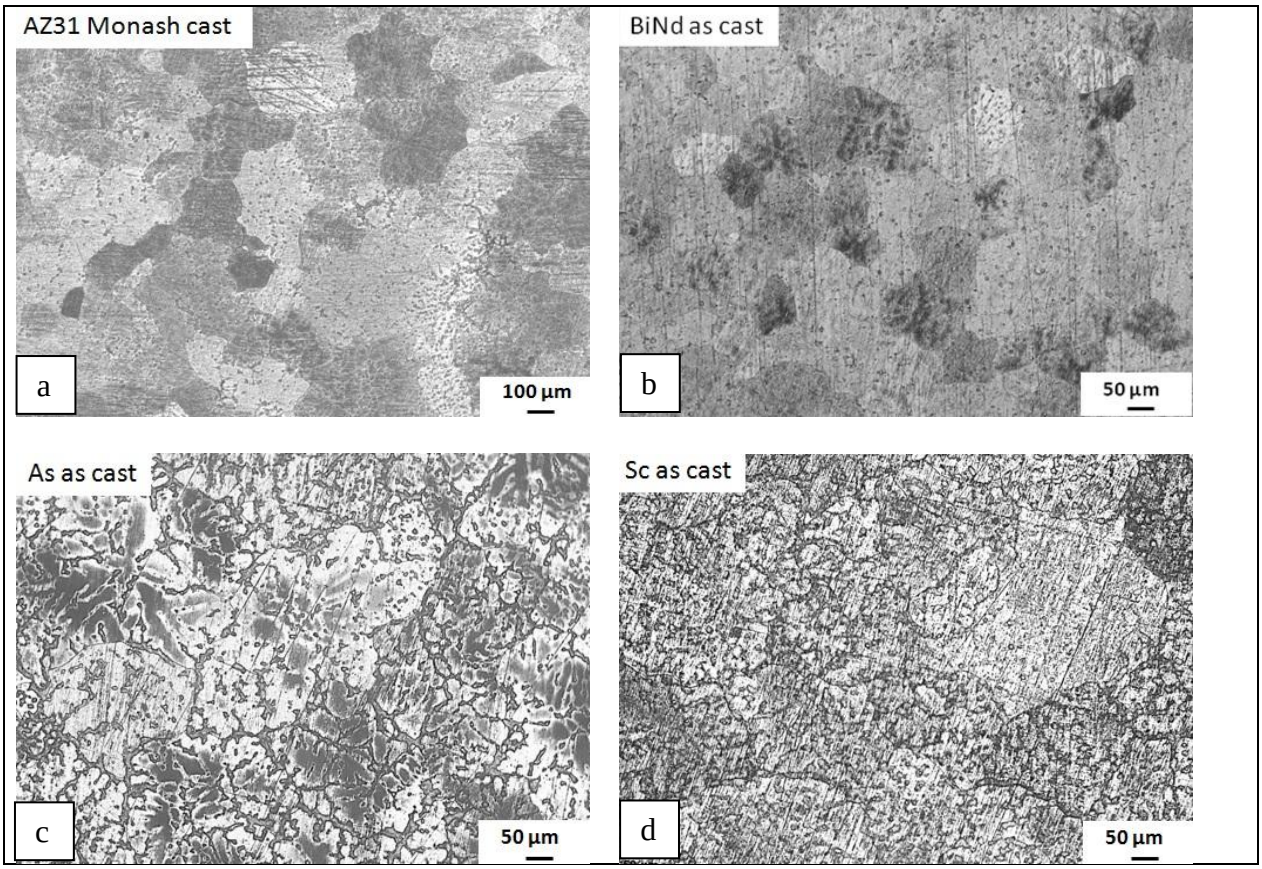

Figure 2. SEM micrographs of the as-cast microstructure for selected alloys: (a) Monash cast AZ31B, (b) BiNd-modified, (c) As-modified, and (d) Sc-modified.

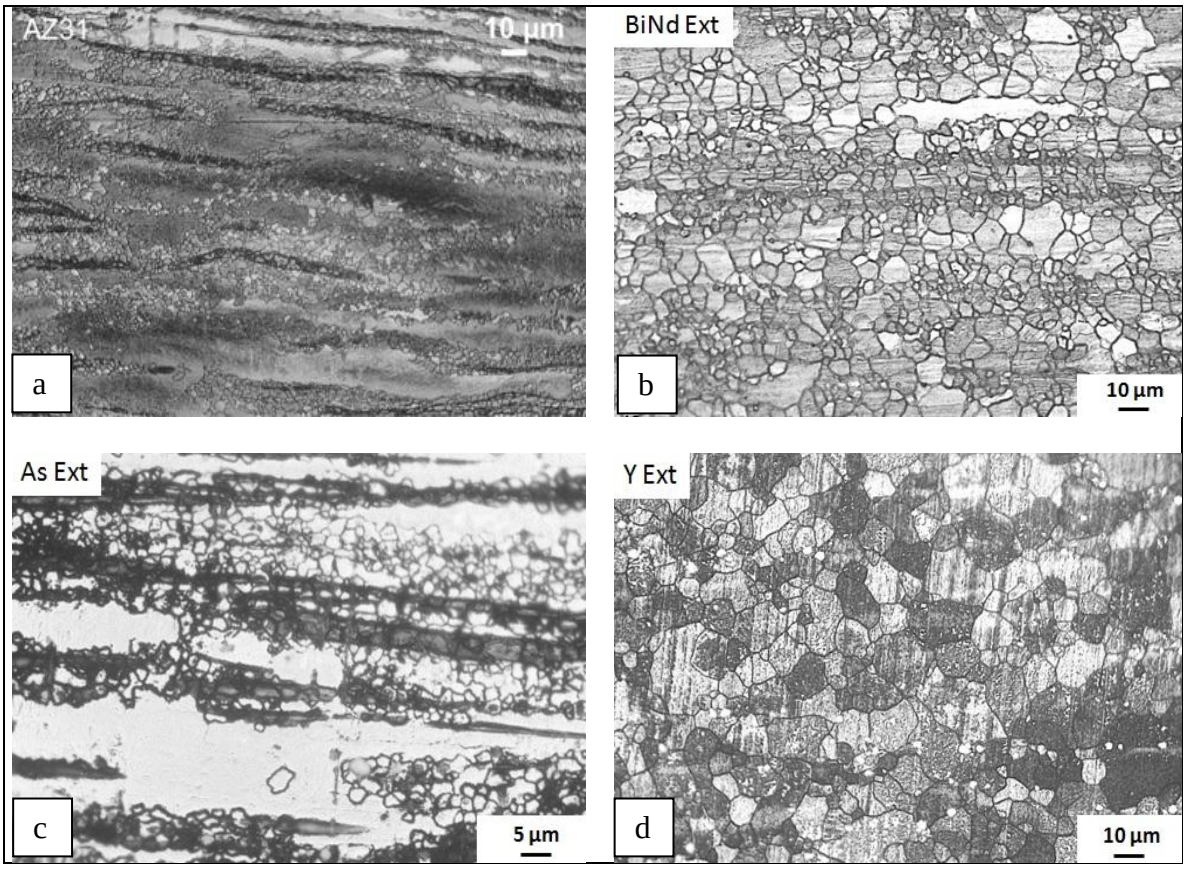

Figure 3. SEM micrographs of the extruded microstructure for selected alloys: (a) Monash-cast AZ31B, (b) BiNd-modified, (c) As-modified, and (d) Y-modified.

Room temperature tensile stress-strain curves are shown in figure 4. In addition, yield strength-elongation pairs are plotted with the alloying element used to identify the respective data point. Obviously, the addition of even small amounts of an additional alloying element can result in significant changes in mechanical performance. Part of the changes in mechanical performance can be attributed to a change in grain size—either an increase or decrease—relative to the parent AZ31B alloy. An additional factor that influences tensile properties is an increase in solid-solution strengthening due to the additional alloying element. Alternatively, in some cases the introduction and/or increase of (brittle) precipitates associated with a particular alloying element (e.g., In, Bi) can result in a reduction in tensile strength and/or total elongation. In addition, the "leaching" of Al from the Mg grains, as suspected in the Y-modified alloy, can result in a significant reduction in mechanical performance. Clearly, there is a complex dependence of mechanical performance on the interaction between grain size, solid-solution strengthening, and precipitate composition/content. This area remains a central focus of ongoing research.

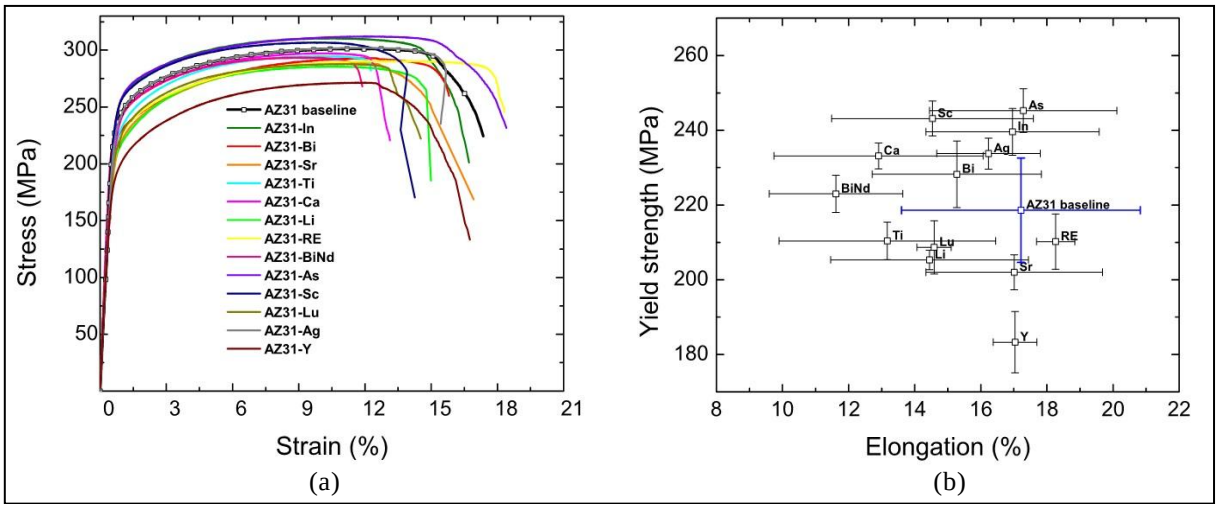

Figure 4. (a) Tensile stress-strain curves for each of the alloys and (b) plot correlating yield strength with total elongation based on added alloying element.

Curves collected from the potentiodynamic polarization tests are given in figure 5a. Potentiodynamic polarization reveals information regarding reaction kinetics, and can therefore be used to evaluate the influence of a particular element on overall anodic and cathodic kinetics. This data is more clearly plotted in figure 5b, which shows corrosion potential (Ecorr) as a function of instantaneous corrosion current (icorr) for each alloying element. Points located up and to the left of the AZ31B point indicate a reduction in anodic dissolution rate, whereas points located down and to the left of AZ31B reflect a reduction in the cathodic reaction rate relative to the base alloy. Although the influence of alloying elements on the corrosion of AZ31B is complex, the addition of more noble elements (such as Bi, In, and Sc) into solid solution will generally result in a reduced anodic dissolution rate. As a higher potential with lower current is the desired property combination, elements such as Lu, As, Sc, and In seem to show promise for improving the corrosion performance of AZ31B.

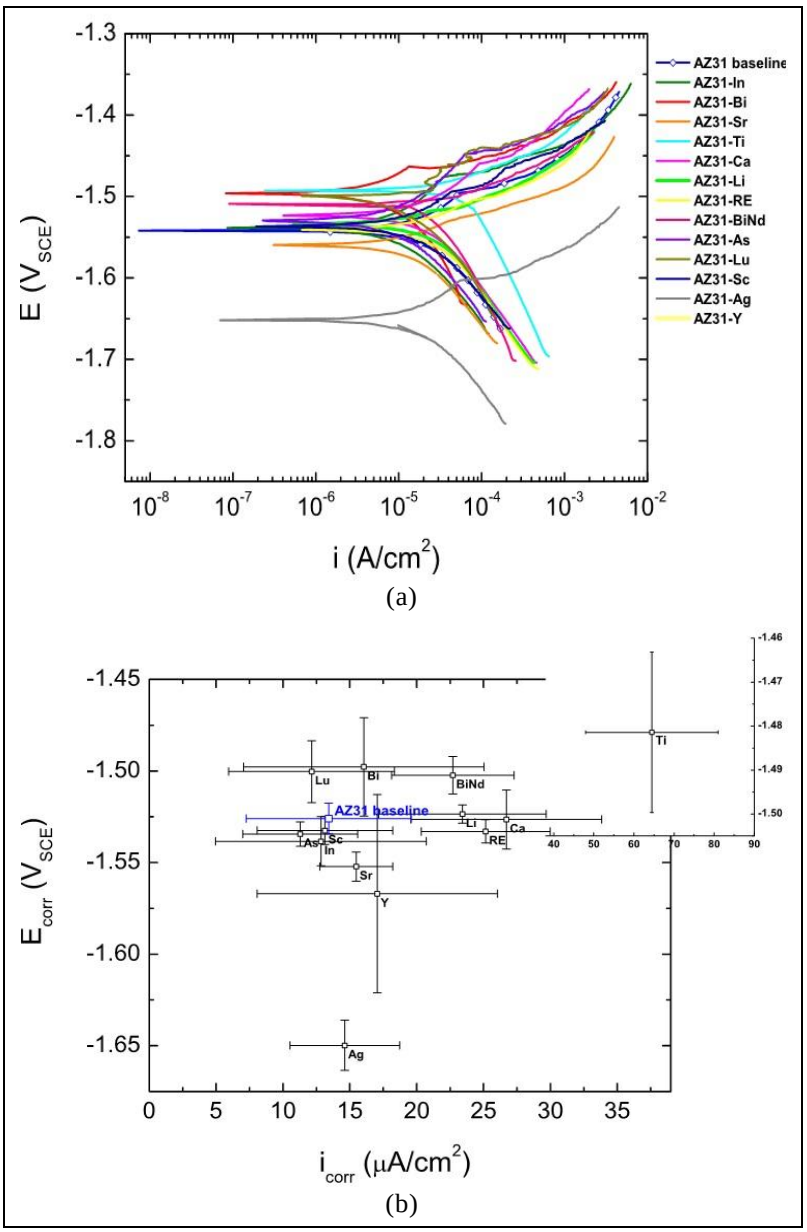

Figure 5. (a) Potentiodynamic polarization curves collected from all alloys, and (b) corrosion potential as a function of corrosion current indicated by alloying element.

Figure 6 shows the correlation between the corrosion rate and mass loss for each of the modified alloys. In general, the difference in mass loss between alloys is minimal. Furthermore, as the mass loss test does not provide any information regarding the actual corrosion mechanism(s), it should be considered as a general, rather than definitive, tool for making observations about the potential corrosion performance of a material.

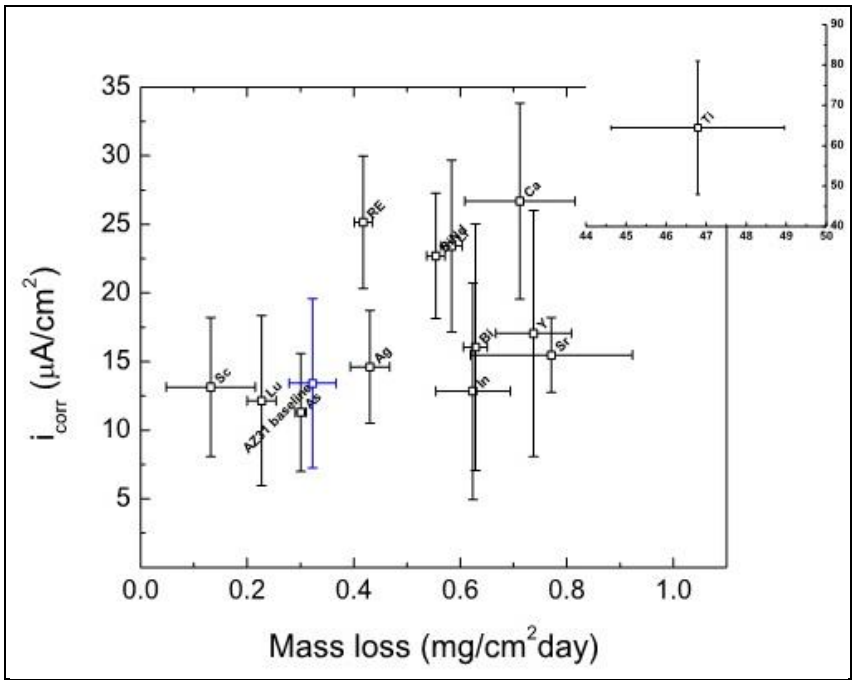

Figure 6. Relationship between corrosion current and mass loss as indicated by alloying element. Except in the case of Ti, the differences in mass loss are minimal.

Shown in figure 7 are two plots that provide insight into the influence of alloying additions on the combined mechanical and physical properties of AZ31B. Taken together, the plots indicate that Sc, As, Ag, and In additions increase the yield strength relative to the AZ31B alloy cast at Monash, with minimal changes in mass loss and overall toughness. Although the addition of Lu appears to improve performance, there is concern about its use due to cost and availability.

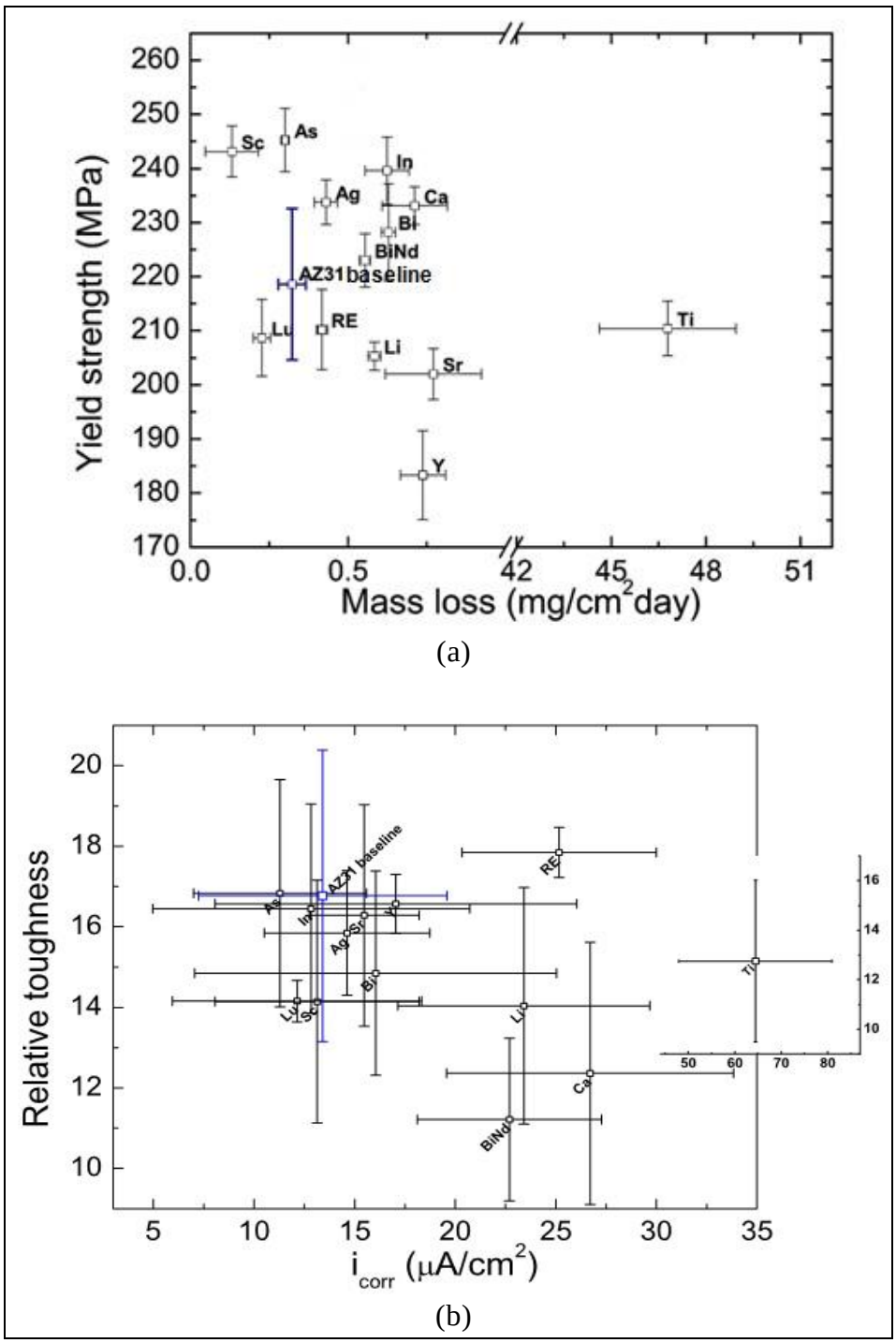

Figure 7. Correlation of (a) yield strength and mass loss, as well as (b) toughness and corrosion current as indicated by the respective alloying element.

The final physical property that was examined for each alloy was the degree of texture, or crystallographic orientation, present in the extruded sample. Because of its hexagonal close packed crystal structure, Mg alloys are well known for their strong tendency to form basal

texture following even a limited degree of working. In Mg, the influence of texture is most readily apparent in the anisotropic mechanical properties. Although other factors, such as precipitates and or second phases can influence alloy response, alloys with more uniform texture (e.g., random orientation) are typically more ductile.

Shown in figure 8(a–d) are inverse pole figures for selected alloys. In general, the alloys display the same trend of maximum intensity located at the common fiber texture position (10-10) for hexagonal metals with c/a ratio of 1.62. This type of orientation is favorable for dislocation slip and twinning. Of the example illustrations, AZ31B has the highest degree of texture, with the Sr-modified showing the lowest degree. Given that the alloys were processed using identical conditions (temperature and extrusion rate), it can be concluded that alloying addition is responsible for the differences in the inverse pole figures. The overall rankings for strongest to weakest texture for all alloys is as follows: Bi, AZ31B, Sc, As, Ag, Lu, In, Ti, Y, Li, Sr, Ca, BiNd, and rare earth-based alloy.

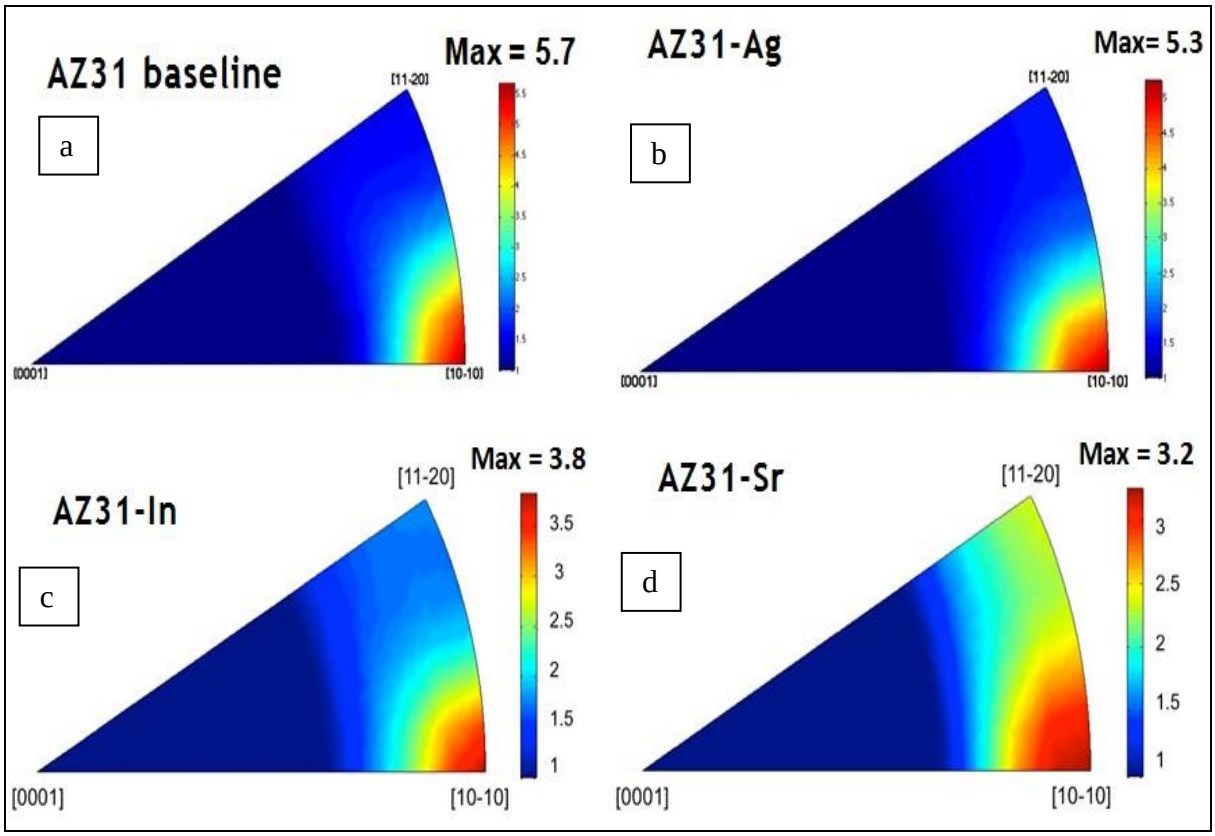

Figure 8. Inverse pole figures indicating the type of texture present in selected alloys: (a) Monash cast AZ31, (b) Ag-modified, (c) In-modified, and (d) Sr-modified.

5. Summary

This report has presented the initial set of findings regarding the influence of atypical alloying elements on the mechanical and electrochemical performance of AZ31B. Alloying elements were selected based on their anticipated potential for improving mechanical performance through solid-solution strengthening, grain refinement, and/or weakening of texture. In addition, it was critical that the chosen elements display little tendency to alter precipitates or otherwise adversely influence the corrosion performance of the base alloy. Based on these considerations, the follow elements were chosen for the study: In, Bi, Sr, Zr, Ti, Ca, Li, Y, Sc, Lu, Ag, and As.

Modified AZ31B ingots containing the desired amount of the alloying addition were cast and then extruded into rods. Subsequent characterization efforts included microscopy, tensile testing, texture measurement, and corrosion testing. Unfortunately, no single element that dramatically improved all properties of interest was found. Of those tested, As, In, Ag, Sc, and Sr were found to provide the best overall improvement in performance by weakening texture, increasing solid solution and/or grain size strengthening, or inhibiting corrosion.

Moving forward, modified alloys containing the down-selected element(s) will be cast and subsequently processed using Equal Channel Angular Extrusion (ECAE) in an attempt to obtain ultra-fine-grained samples. Detailed evaluation of these samples will be conducted to determine the combined effect of grain size and minor alloying additions on mechanical and electrochemical performance. As warranted, ballistic testing will be performed on plate samples ($6 \times 6 \times 1/2$ in or $12 \times 12 \times 1$ in) produced using ECAE facilities available at ARL.

NO. OF COPIES	ORGANIZATION
1 (PDF)	DEFENSE TECHNICAL INFORMATION CTR DTIC OCA
1 (PDF)	DIRECTOR US ARMY RESEARCH LAB IMAL HRA
1 (PDF)	DIRECTOR US ARMY RESEARCH LAB RDRL CIO LL
1 (PDF)	GOVT PRINTG OFC A MALHOTRA
3 (PDF)	DIR USARL RDRL WMM C J LABUKAS B PLACZANKIS RDRL WMM F V HAMMOND